Available online at www.sciencedirect.com
ScienceDirect
International Journal of Heat and Fluid Flow 29 (2008) 269–280
International Journal of HEAT AND FLUID FLOW
www.elsevier.com/locate/ijhff

Pumping and mixing in a microchannel using AC asymmetric electrode arrays

Myung Sup Yoon, Byoung Jae Kim, Hyung Jin Sung *

Department of Mechanical Engineering, Korea Advanced Institute of Science and Technology, 373-1 Guseong-dong, Yuseong-gu, Daejeon 305-701, Republic of Korea

Received 20 July 2007; received in revised form 9 October 2007; accepted 20 October 2007
Available online 3 December 2007

Abstract

A numerical study of electroosmotic microchannel flow driven by arrays of AC (alternating current) asymmetric electrodes was carried out. By installing asymmetric electrode arrays on the top and bottom walls of the microchannel, pumping and mixing flow modes can be generated. The 'pumping mode' (*P*) is generated when the sequences of asymmetric electrode pairs (narrow to wide) on the top and bottom walls are in phase, whereas the 'mixing mode' (*M*) is generated by switching the sequence of electrode pairs of the top wall (e.g., wide to narrow). By combining mixing and pumping modes, enhanced mixing performance can be achieved without significantly reducing the flow rate. Among various combinations of *P* and *M* modes, the alternating *PM* mode showed the best mixing performance due to the iterative convergent and divergent flow motions. The effects of Peclet number and channel height on the mixing efficiency were analyzed in detail.

Keywords: AC electroosmotic flow; Microchannel flow; Asymmetric electrode; Pumping and mixing; Pumping mode; Mixing mode; Mixing efficiency

1. Introduction

Over the past decades, progress in manufacturing techniques for micro-electromechanical systems (MEMS) has enabled the fabrication of various 'lab-on-a-chip' devices or micro total analysis systems (μTAS) (Stone et al., 2004; Nguyen and Wereley, 2003; Li, 2004). In most microfluidic systems, pressure force is required to transport solutions and samples inside a microchannel. Many pumping systems have been developed, including micromechanical pumping (van Lintel, 1988), electrowetting (Beni and Tenan, 1981), thermocapillary pumping (Kataoka and Troian, 1999), electroosmotic pumping (Manz et al., 1994) and electrohydrodynamic pumping (Fuhr et al., 1992). Among the methods developed to date, electroosmosis provides an attractive means of pumping in microfluidic devices. Electroosmosis refers to the movement of excess counterions in the diffuse layer of an electrical double layer (EDL) under an applied electric field. An EDL is composed of a compact layer (or Stern layer) near the charged surface and a diffuse layer outside the compact layer. The net charge in the EDL should balance the charge at the wall surface. Hence, the compact layer contains immobile, surface-attached counterions, whereas the diffuse layer contains mobile counterions with a Poisson–Boltzmann potential distribution. Movement of the counterions in the diffuse layer is induced by applying an electric field; when the counterions move, the surrounding liquid molecules also move due to the viscous effect.

The majority of studies on electroosmotic flow have focused on the direct current (DC) case, in which a DC electric field is applied across a pair of electrodes installed at either end of a channel in order to pump fluid. However, DC electroosmotic flow has drawbacks such as the need for a large voltage input, typically in the kilovolts range. Researchers have begun to examine a new type of fluid flow induced by application of an alternating current (AC)

* Corresponding author. Tel.: +82 42 869 3027; fax: +82 42 869 5027.
E-mail address: hjsung@kaist.ac.kr (H.J. Sung).

0142-727X/$ - see front matter © 2007 Elsevier Inc. All rights reserved.
doi:10.1016/j.ijheatfluidflow.2007.10.002

(Ramos et al., 1999; Green et al., 2000, 2002; González et al., 2000). This AC electroosmosis method has the merit of low AC voltage input. Theoretical and experimental studies have examined how fluid circulation can be created over a co-planar symmetric AC-powered electrode, and have analyzed the induced charge in the electrical double layer on the electrode surface. Those studies indicated that the physical mechanism responsible for the circulating fluid motion is the force exerted on the electrical double layer by a tangential electric field. However, this method was unable to produce a net flow over an entire electrode array. Later, Ajdari (2000) suggested that a net pumping flow can be achieved using an array of asymmetric electrodes, and Brown et al. (2000) confirmed this hypothesis experimentally. Brown et al. explained the net pumping flow by a non-zero time averaged electroosmotic slip velocity originating from the asymmetric electric field. Following this work on the physical mechanism underlying pumping flow, Ramos et al. (2003) showed the dependency of pumping on voltage, AC frequency and electrode disposition. These parameter studies were completed by Olesen et al. (2006), who generated new data and identified the optimal specifications that give maximum pumping. In addition, Olesen et al. (2006) studied the effects of confined geometry, Faradaic current injection and nonlinear Debye layer capacitance in an effort to understand experimental results that conflicted with theory, such as the reversal of the pumping direction when the driving voltage and frequency became sufficiently high.

Previous studies of AC electroosmotic flow using asymmetric electrode arrays have mainly focused on the flow pumping mechanism. Recently, many studies have examined mixing, applying AC to various electrode designs. Lastochkin et al. (2004) proposed a mixer based on AC Faradaic polarization and observed electroosmotic flow for electrolyte with high conductivity. Squires and Bazant (2004) and Bazant and Squires (2004) utilized induced-charge electroosmotic flow for mixing, by installing asymmetric conducting posts or conducting strips at the side walls. Zhao and Bau (2007) introduced a stirrer concept to prompt chaotic advection utilizing induced-charge electroosmosis.

In the present study, we examine a channel in which arrays of asymmetric electrodes are installed on the top and bottom plates. By adjusting the sequence of asymmetric electrode pairs (narrow and wide electrodes during one period) on the top wall, pumping and mixing flow modes can be simultaneously generated in the channel. Emphasis is placed on the sequence of asymmetric electrode pairs on the top wall in reference to the sequence on the bottom wall. When the sequence of the electrode pairs on the top wall is the same as that on the bottom wall (e.g., narrow to wide during one period), a pumping flow is generated between the two walls. When, however, the sequence of the electrode pairs on the top wall does not match that on the bottom wall (e.g., wide to narrow on the top wall, and narrow to wide on the bottom wall), a mixing flow is generated. Hereinafter, these two flow patterns are referred to as the 'pumping mode' (P) and 'mixing mode' (M), respectively. The pumping mode alone does not mix species effectively and the mixing mode alone does not transport species well. We test various combinations of pumping and mixing modes to determine the optimal design in terms of the mixing efficiency and pumping flow rate. A detailed flow analysis is performed to clarify the pumping and mixing modes.

2. Numerical procedure

A schematic diagram of the geometrical layout of the channel used in the present work is given in Fig. 1. The two-dimensional infinite electrically insulating substrate contains a periodic array of asymmetric electrode pairs at the top wall and another such array at the bottom wall. An alternating voltage of opposite sign $(-V^*, +V^*)$ with frequency ω^* is applied to each pair of narrow and wide electrodes. Each electrode pair in the array consists of a narrow electrode of length W_1^* and a wide electrode of width W_2^* separated by a narrow gap G_1^* and a wide gap G_2^*, respectively. The notation for the length and gap size $(W_1^*, W_2^*, G_1^*, G_2^*)$ is the same as in previous studies (Ramos et al., 2003; Olesen et al., 2006). The height of the channel is H^* and the period of the electrode array is L^* $(= W_1^* + G_1^* + W_2^* + G_2^*)$. The origins of the arrays are x_T^* and x_B^* at the top and bottom walls, respectively.

The non-dimensional electrical potential (ϕ) in the bulk electrolyte satisfies Laplace's equation, and the harmonic time dependency of ϕ can be dealt with using the complex variable expression $\hat{\phi}$. For the electric potential field, the governing equation and boundary conditions are

$$\begin{aligned} &\nabla^2\hat{\phi} = 0 \\ &\vec{n}\cdot\nabla\hat{\phi} = \mathrm{i}\omega(\hat{\phi}+1), \quad \text{at the narrow electrode} \\ &\vec{n}\cdot\nabla\hat{\phi} = \mathrm{i}\omega(\hat{\phi}-1), \quad \text{at the wide electrode} \\ &\vec{n}\cdot\nabla\hat{\phi} = 0, \quad \text{at the glass substrate} \end{aligned} \tag{1}$$

For the microsystem in which the viscous term dominates the inertia term, the Stokes equation governs the fluid. The Reynolds number, $Re(\equiv \frac{U_0^* G_1^*}{\nu^*})$ is about 0.1 in the present study. The time averaged electroosmotic slip velocity is applied at the electrode and the no-slip conditions at the non-electrode surfaces are

$$\begin{aligned} &\nabla\cdot\vec{u} = 0, \quad -\nabla p + \frac{1}{Re}\nabla^2\vec{u} = 0 \\ &\langle u_s\rangle = -\frac{1}{4}\partial_x|\hat{\phi}\pm 1|^2, \quad \text{at the narrow and wide electrode} \end{aligned} \tag{2}$$

Periodic boundary conditions at the inlet and outlet of the channel are applied for the electric potential and flow fields.

The species equation is solved to understand the mixing effects:

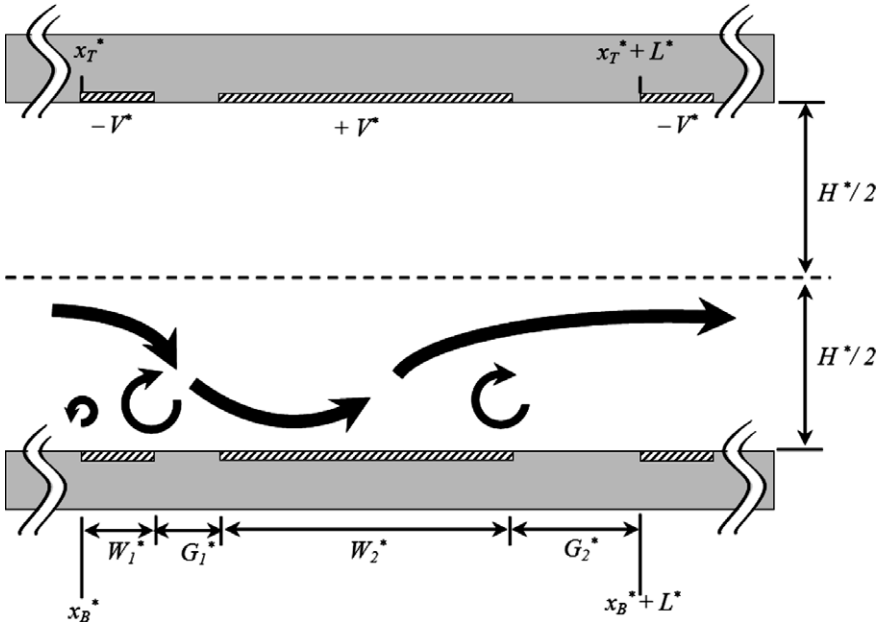

Fig. 1. Sketch of the device geometry.

$$\begin{aligned}
&\vec{u}\cdot\nabla c = \frac{1}{Pe}\nabla^2 c \\
&\vec{n}\cdot\vec{j} = 0, \quad \text{at the impermeable surface} \\
&c = 1 \text{ and } 0, \quad \text{at the inlet} \\
&\quad (0 \leqslant y \leqslant 0.5H \text{ and } 0.5H \leqslant y \leqslant H) \\
&\vec{n}\cdot\nabla c = 0, \quad \text{at the outlet}
\end{aligned} \tag{3}$$

where $\vec{j}$ is the mass flux vector, which is the sum of the diffusive flux and convective flux ($\vec{j} = -\frac{1}{Pe}\nabla c + c\vec{u}$). We assume that all mass passing through the outlet is convection-dominated. Since the non-dimensional parameter, the Peclet number ($Pe(\equiv \frac{U_0^* G_1^*}{D^*})$) is of the order of up to 10^4, the convective term in Eq. (2) cannot be neglected. As for the mixing analysis, time-dependent terms are important. However, when the time scale of the AC forcing is much smaller than those of the advection and diffusion terms, time-dependent terms are negligible. The fluid flow by AC electroosmotic occurs at the order of kHz in general. In such low frequencies ($\omega = 2\pi f \leqslant \sigma^*/\varepsilon^*$), the double layer fully develops in phase with the applied field (Squires and Bazant, 2004). The AC electroosmotic flow thus can be considered to be steady.

The above non-dimensional governing equations and boundary conditions are derived using the characteristic parameters summarized in Table 1. The values of the geometrical parameters (W_1, G_1, W_2, G_2) employed were those of Mpholo et al. (2003). All length scales were non-dimensionalized by the characteristic length G_1^*. The working fluid in the channel was a 10^{-4} M KCl solution with conductivity σ^* and permittivity ε^*. The characteristic velocity and voltage in Table 1 are high to be used in the standard linear model. In general, the standard model estimates the velocity slightly higher than the experimental value because it does not cover Faradaic currents, nonlinear Debye layer capacitance and steric effects of the ions in the Debye layer (Kilic et al., 2007). In the present study, however, we used the standard model to predict the flow qualitatively. Following Ramos et al. (2003), we assumed that the applied voltage was small and the frequency low in order to prevent electrolysis of the electrolyte and an ionic non-equilibrium state of the Debye double layer. The above system of equations was solved using the finite element method with a triangular mesh, in conjunction with the direct LU factorization of the sparse matrix solver (Davis and Duff, 1997).

Table 1
Characteristic parameters of the electrokinetic system for a 10^{-4} M KCl working electrolyte at 15 °C

Characteristic length	G_1^*	5 μm
Debye length	λ_d^*	30 nm
Electrical conductivity	σ^*	0.001207 S/m
Permittivity	ε^*	7.264×10^{-10} F/m
Dynamic viscosity	μ^*	0.001139 Pa s
Capacitance ratio	δ	0.1
Applied voltage	V^*	0.415 V
Applied frequency	$\omega[\equiv G_1^*\varepsilon^*\omega^*/\sigma^*(1+\delta)\lambda_d^*]$	1.26
Characteristic velocity	$U_0^*[\equiv \varepsilon^* V^{*2}/\mu^* G_1^*(1+\delta)]$	0.02 m/s
Geometric length	G_1, W_1, G_2, W_2	1, 1, 3, 5

3. Results and discussion

Fig. 2 shows the time averaged slip velocities at the narrow and wide electrodes obtained in the present simulations, along with those calculated by Olesen et al. (2006). The geometry (W_1, G_1, W_2, G_2) and frequency (ω) are the same as those of Olesen et al. (2006). The time averaged

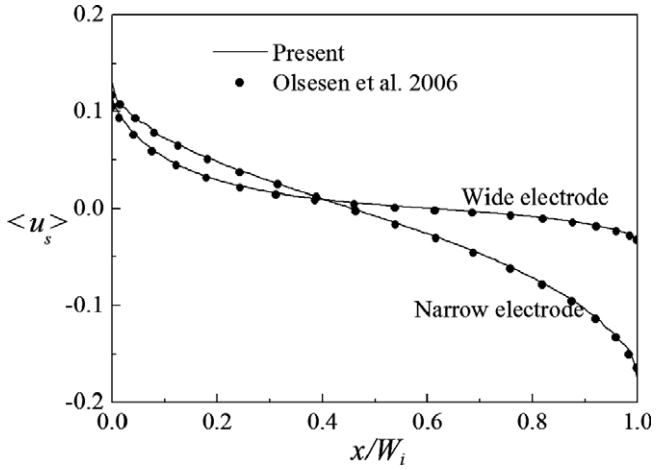

Fig. 2. Validation of the present simulation. The geometry (W_1, W_2, G_1, G_2) and frequency (ω) are same as those of Olesen et al. (2006).

slip velocity of the narrow electrode is more symmetric than that of the wide electrode, which gives a smaller pumping effect. Our data are in excellent agreement with those of Olesen et al. (2006), which validates the numerical schemes for the potential and flow fields. Throughout the present study, the maximum number of mesh points is about 18,000, which is shown to be enough to solve the species equation for high $Pe = 10^4$.

The flow patterns of representative pumping and mixing modes are represented in Fig. 3. As mentioned above, when the sequence of the electrode pairs on the bottom wall is aligned with that on the top wall, i.e., the sequence (W_1, G_1, W_2, G_2) during the period L, the pumping mode is formed. An asymmetric time averaged slip velocity of positive value is generated over the wide electrode, which corresponds to the flow moving from left to right. However, if the sequence of the electrode pairs on the top wall is switched to (W_2, G_1, W_1, G_2), the mixing mode is generated. In this mode, large circulation cells form between the top and bottom walls that enhance mixing. These circulation cells in the mixing mode become clearer as the channel height decreases $(H = 10, 5, 2)$.

Fig. 4 shows cross-sectional views of the velocity profiles at $\alpha\beta$ and $\alpha'\beta'$ in Fig. 3. At the pumping mode in Fig. 4a, the flow seems to become activated as the channel height (H) decreases. At $H = 2$, the velocity profile is parabolic with a single peak velocity at the centerline, which may give maximum pumping. As the channel height is increased, however, many local peak velocities appear. These data indicate that effective pumping occurs at the small channel height $(H = 2)$ for a given slip velocity. In a manner similar to the pumping mode, maximum mixing occurs in the channel with a small height. Inspection of the velocity as a function of distance along the channel (Fig. 4b) reveals greater velocity fluctuations in the $H = 2$ system than in the system with a channel of height $H = 10$. However, regardless of the benefits of flow activation, the small channel height may restrict the flow through the channel. One of the main objectives in microchannel design is to maximize sample transportation, which is related to the surface flow rate $(Q = \int u\,dh)$. As noted by Olesen et al. (2006), Q is proportional to the channel height if the dimensionless velocity profile is identical. For example, in the present work the flow rates for the three channel heights, $H = 10$, 5 and 2, are $Q = 0.0336$, 0.0186 and 0.0099, respectively.

The effects of shifting the positions of the top and bottoms walls with respect to one another are shown in Figs. 5 and 6 for the mixing mode and in Fig. 7 for the pumping mode. In these simulations, the original electrode geometry

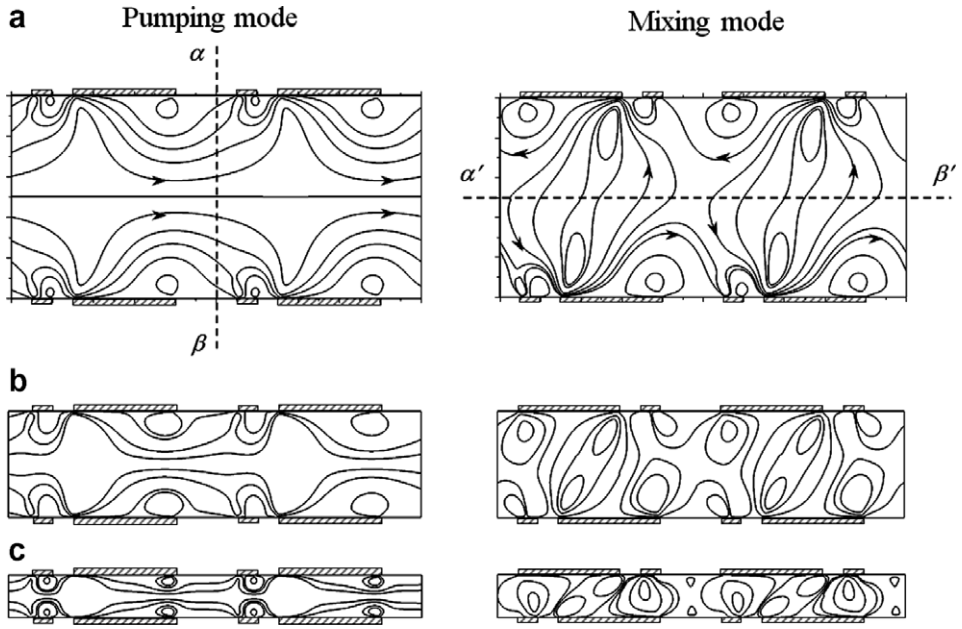

Fig. 3. Flow patterns of the pumping and mixing modes for different channel heights. (a) $H = 10$, (b) $H = 5$ and (c) $H = 2$.

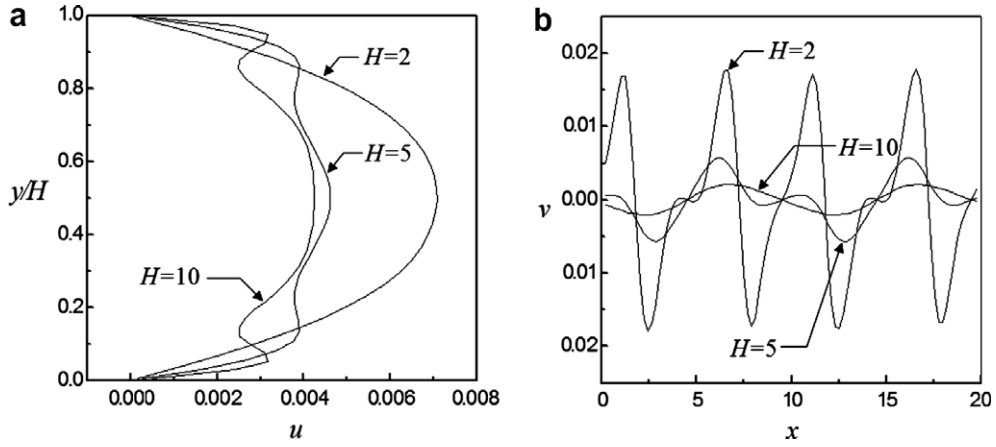

Fig. 4. Velocity profiles. (a) Pumping velocity profiles through $\alpha\beta$ and (b) mixing velocity profiles through $\alpha'\beta'$ in Fig. 3.

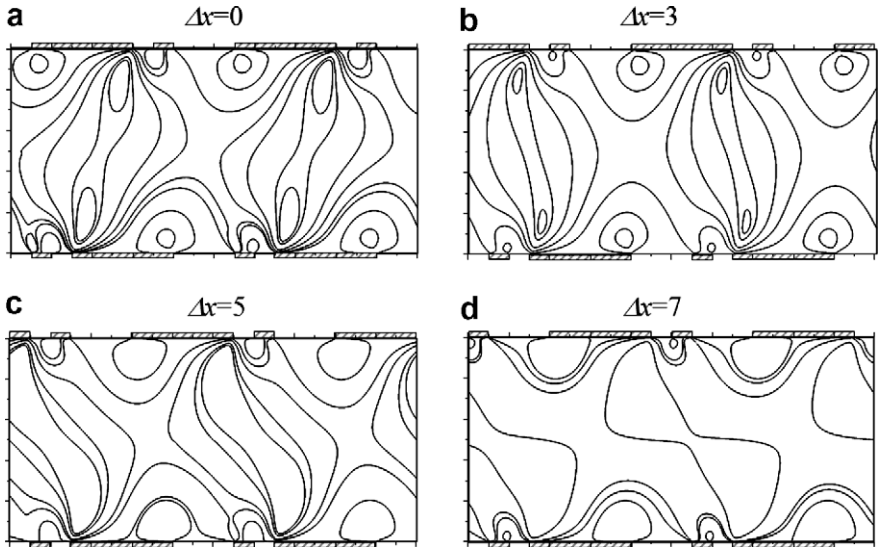

Fig. 5. Flow patterns of the mixing mode for different Δx.

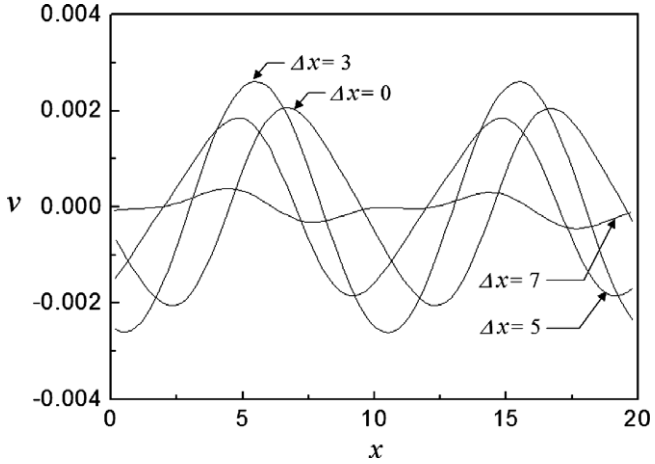

Fig. 6. Velocity profiles for different Δx.

and channel height were fixed at $W_1, W_2, G_1, G_2 = 1, 5, 1, 3$ and $H = 10$, and the position of the top wall was shifted a distance $\Delta x(=x_B - x_T)$ relative to the bottom wall. For the mixing mode, the shape of the circulation cell is gradually distorted as Δx increases, with the maximum distortion occurring at $\Delta x = 7$ (Fig. 5). If Δx is increased further (e.g., to $\Delta x = 10$), the circulation cell becomes less distorted because the period of the electrode array is $L = 10$. The variation in flow velocity with downstream distance in the mixing mode is shown in Fig. 6. The velocity profiles at $\Delta x = 3$ and 5 do not deviate significantly from the profile at $\Delta x = 0$. At $\Delta x = 7$, however, the distorted cell prevents mixing and the velocity profile is disrupted. Fig. 7 shows the flow patterns for different Δx for the system in the pumping mode. The main target of the pumping mode is to maximize the flow rate under a given set of conditions. As denoted in the upper right part of Fig. 7, the flow rate is almost the same regardless of Δx, indicating that shifting

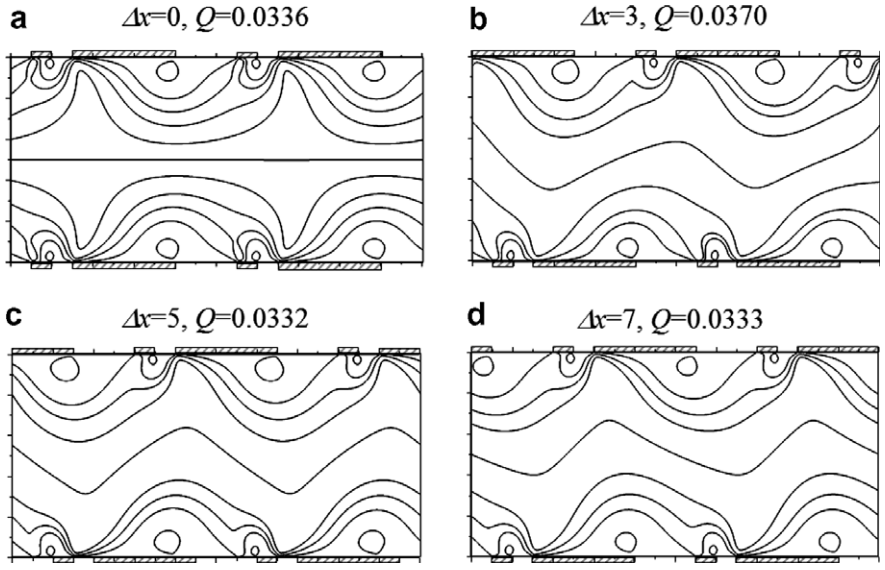

Fig. 7. Flow patterns of the pumping mode for different Δx.

the top and bottom walls with respect to one another has little effect on the pumping mode. For convenience, below we consider the case of $\Delta x = 0$ when testing the pumping mode.

A measure of the mixing efficiency should be defined in order to clarify the mixing performance. In the present study, the mixing efficiency is defined as

$$e_x \equiv \left(1 - \frac{\int |c(y) - c_\infty| \mathrm{d}y}{\int |c_0 - c_\infty| \mathrm{d}y}\right) \times 100\% \tag{4}$$

where $c(y)$ is the species concentration profile across the channel height, c_0 is the concentration at the unmixed inlet, and c_∞ is the concentration in the completely mixed state (0.5) (Li, 2004). Since the species mixing is expressed by the non-dimensional parameter Pe, known as the Peclet number, we analyzed the effect of Pe on the mixing. For a fixed velocity (U_0^*) and length scale (G_1^*) (see Table 1 for the values used), a large diffusivity D^* means a small Pe. The concentration distributions obtained for three different Pe values are displayed in Fig. 8b–d, respectively, for the pumping mode shown in Fig. 8a. At the inlet, the lower half of the flow has a concentration of 1 (white) and the upper half a concentration of 0 (black). As Pe increases, the mixing efficiency (e_o) at the outlet decreases. For $Pe = 10^2$, the flow is almost completely mixed (mixing efficiency, $e_o = 97\%$), whereas the mixing is poor in the system with $Pe = 10^4$ ($e_o = 14.6\%$). Since the typical species diffusivity falls between $O(10^{-10})$ and $O(10^{-11})$, hereafter we fix the Pe value at $Pe = 10^4$.

Mixing inside the channel can be enhanced by selecting an appropriate combination of pumping and mixing

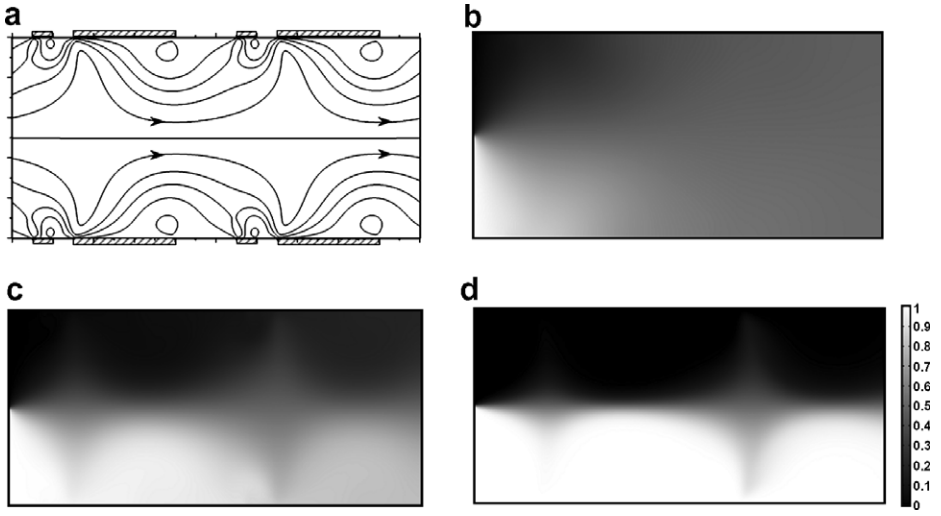

Fig. 8. Streamlines and concentration distributions for the pumping mode. (a) Streamlines, (b) $Pe = 10^2$, $e_o = 97.0\%$, (c) $Pe = 10^3$, $e_o = 55.4\%$ and (d) $Pe = 10^4$, $e_o = 14.6\%$.

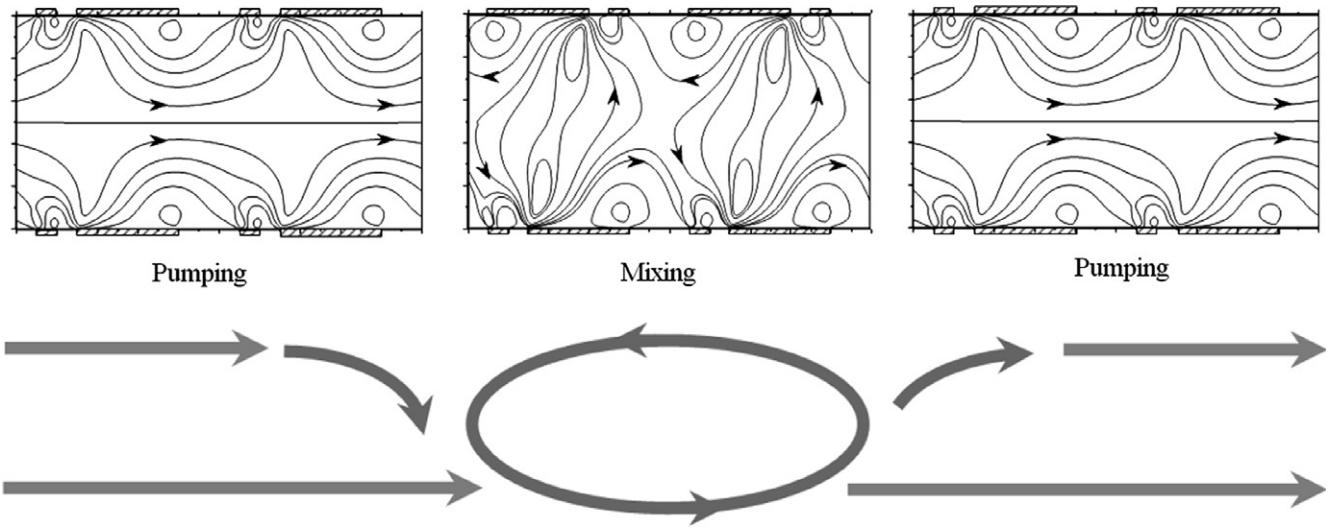

Fig. 9. Conceptual flow models for *PPMMPP*.

modes. Fig. 9 shows a conceptual flow structure in which two mixing modes are placed in the middle of four pumping modes (*PPMMPP*). The mixing mode acts as a stirring wheel and causes congestion that inhibits pumping. For the concrete realization of this concept, we simulated various combinations of pumping and mixing modes. Here we use the notation P_pM_m to denote a combination of p consecutive pumping modes followed by m consecutive mixing modes; the total number of modes in such a system is therefore $p+m$. For example, the system with four consecutive pumping modes and no mixing modes, P_4, has a flow rate $Q=0.035$ and a mixing efficiency $e_o=21.5\%$, as shown in Fig. 10a. If the last two pumping modes are replaced by mixing modes to give P_2M_2 (Fig. 10b), the mixing efficiency increases three-fold and the flow rate is halved. These trends are supported by the variations in the flow rate and mixing efficiency as a function of the fraction of modes that are mixing modes $[m/(p+m)]$, shown in

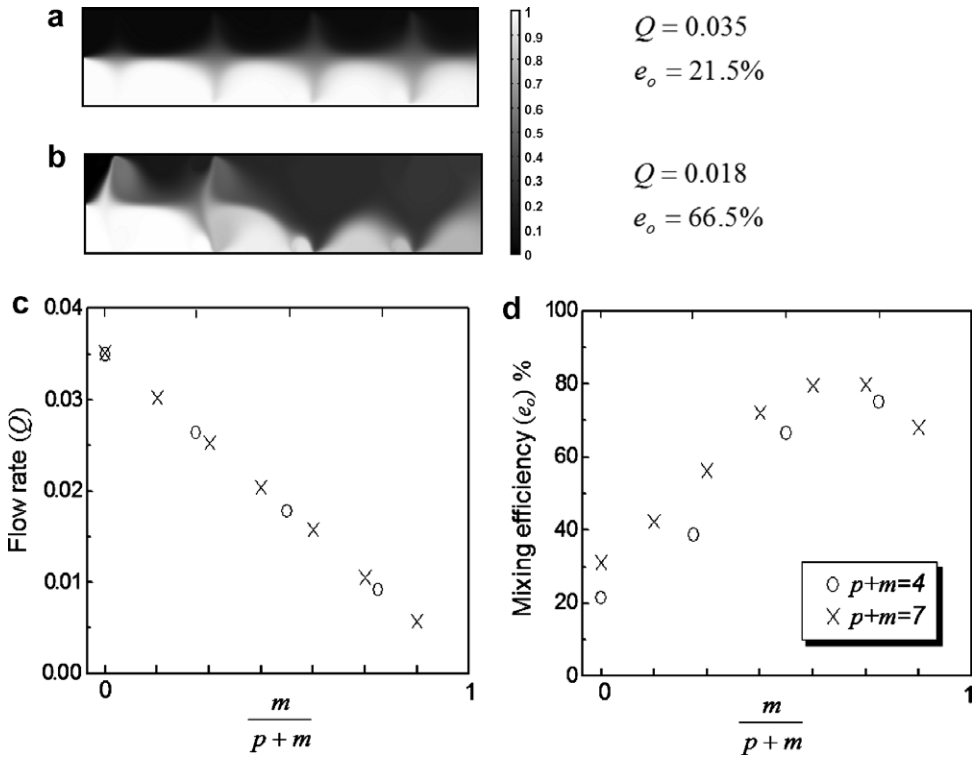

Fig. 10. Flow rates and mixing efficiencies for P_pM_m at $Pe=10^4$ and $H=10$. (a) Concentration for P_4, (b) concentration for P_2M_2, (c) flow rate and (d) mixing efficiency.

Fig. 10c and d, respectively. As the proportion of mixing modes $[m/(p+m)]$ increases, the flow rate $(Q = \int u\,dh)$ decreases linearly and the mixing efficiency (e_o) increases up to a maximum of 80%. When the proportion of mixing modes increases beyond a certain value, however, the mixing efficiency decreases because a very large proportion of mixing modes prohibits pumping and hinders rather than enhances mixing.

Fig. 11 shows the mixing flow patterns obtained for two different combinations of two consecutive mixing modes, MM and MM', where M is a normal counterclockwise circulating mixing mode and M' is a clockwise circulating mixing mode created by switching the top and bottom electrode arrays. For the original MM combination (Fig. 11a), the main flow passes below the secondary circulating flow. Hence, the concentration (Fig. 10b) and the main streamlines (Fig. 12a) are biased to the bottom wall and the flow exhibits a bouncing motion over the bottom plate. For the combination MM' (Fig. 11b), by contrast, the main flow passes across the center of the channel as it encounters the clockwise circulation. The streamlines in Fig. 12 clearly reflect the conceptual model. Twenty streamlines start at the inlet of each channel. During the first two pumping modes, almost symmetric diverging and converging flow patterns are observed. At the first mixing mode, however, the streamlines immediately bounce over the bottom wall for the system with consecutive normal mixing modes MM (Fig. 12a), but exhibit a zigzag motion for the MM' mode (Fig. 12b). The mixing efficiencies and the corresponding flow rates for several combination modes are summarized in Table 2.

As is clear from the streamline patterns in Fig. 12, mixing occurs via several mechanisms (Li, 2004). First, mixing occurs due to the convective circulating motion in the mixing mode. Second, forcing the main flow through a narrow channel significantly increases the local concentration gradients, leading to a greater diffusive flux and thus to enhanced mixing. A third factor contributing to mixing is the diverging flow motion that occurs during the pumping mode or occurs at the end of the mixing mode (see Fig. 12).

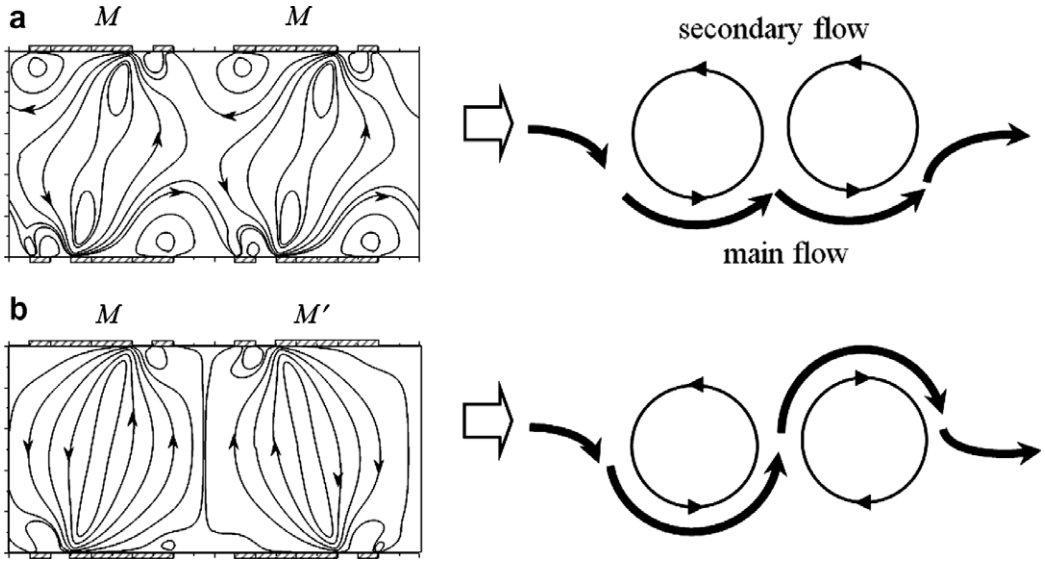

Fig. 11. Two mixing modes. (a) MM and (b) MM'.

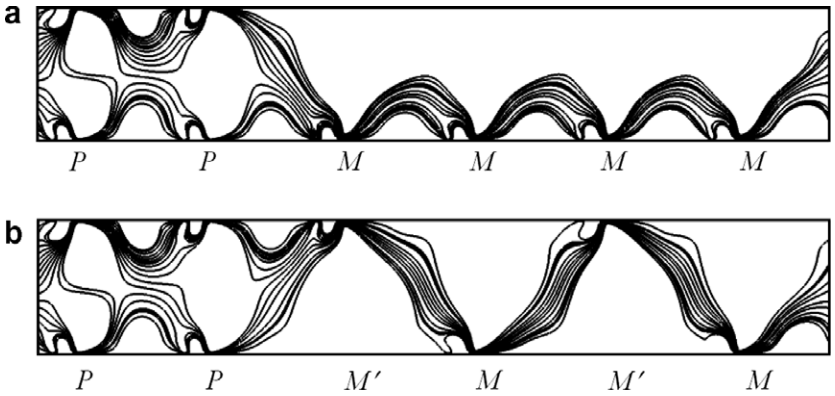

Fig. 12. Streamlines for (a) $PPMMMM$ and (b) $PPM'MM'M$.

Table 2
Performance evaluations for various combinations of the pumping and mixing modes at $H = 10$ and $Pe = 10^4$

	Q	e_o %
p+m = 4		
PPPP	0.0351	21.5
PPPM	0.0264	38.8
PPMM	0.0178	66.5
PMPM	0.0173	75.0
PMMP	0.0163	67.1
PMMM	0.0092	75.1
PMM′M	0.0088	64.2
p + m = 7		
PPPPPPP	0.0351	31.1
PPPPPPM	0.0302	42.3
PPPPMMM	0.0203	72.1
PPMMMPP	0.0202	74.2
PPMM′MPP	0.0203	79.5
PMMMMMP	0.0104	91.9
PMM′MM′MP	0.0110	85.6
PMPMPMP	0.0201	80.6

The concentration distributions in Fig. 13 and the mixing efficiency curves in Fig. 14 reflect these mixing mechanisms. The system comprised of seven consecutive pumping modes (Fig. 13a) has a flow rate of $Q = 0.0351$ and a mixing efficiency of $e_o = 31.1\%$. However, on replacing the middle three pumping modes with mixing modes, to give $P_2M_3P_2$ (Fig. 13b), the mixing efficiency increases drastically to $e_o = 74.2\%$ without a critical loss of flow rate ($Q = 0.0202$). The use of alternating PM modes gives even better performance, i.e., $e_o = 80.6\%$ (Fig. 13c). Note that the flow rates of the $P_2M_3P_2$ and $PMPMPMP$ systems (Fig. 13b and c) are almost the same. Fig. 14 shows the mixing efficiency along the channel for the above three systems: P_7, $P_2M_3P_2$ and $PMPMPMP$. For all three systems,

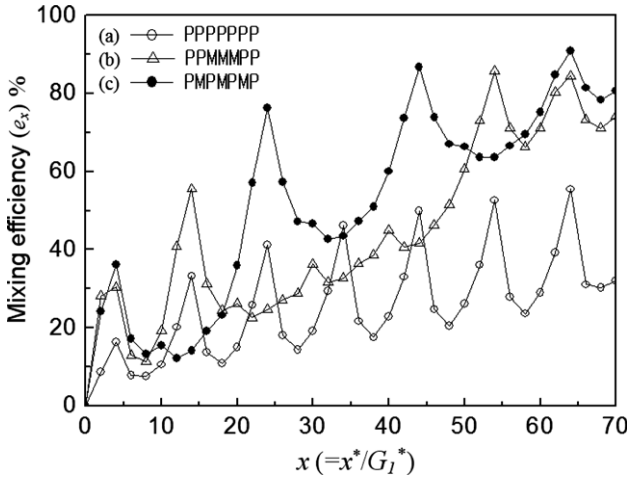

Fig. 14. Mixing efficiency along the channel.

the mixing efficiency shows oscillatory motions, with the average mixing efficiency increasing monotonically. In the oscillatory patterns, the points of local maximum mixing efficiency coincide with the pumping mode positions, where the narrow width of the main stream rapidly diverges. The alternating PM mode shows good mixing performance throughout the entire calculation domain.

The effects of the Peclet number and channel height (H) on the mixing efficiency (e_o) for the pure pumping mode (P_7) are presented in Fig. 15. At a given channel height (H), mixing performance increases with decreasing Pe. As the channel height decreases ($H = 20$, 10 and 5), a mixing efficiency of 90% is achieved even at large Pe ($Pe = 200$, 1000 and 7000, respectively). Systems with smaller channel heights exhibit better mixing performance because they have a large concentration gradient across the channel height, which induces a strong diffusive flux. The mixing

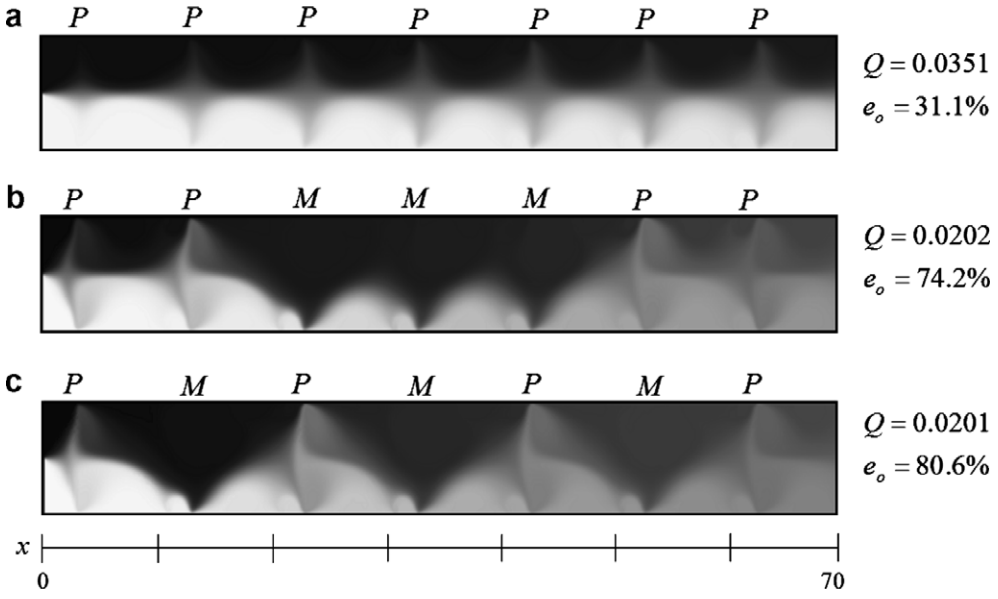

Fig. 13. Concentration distributions with various combinations of pumping and mixing at $Pe = 10^4$ and $H = 10$.

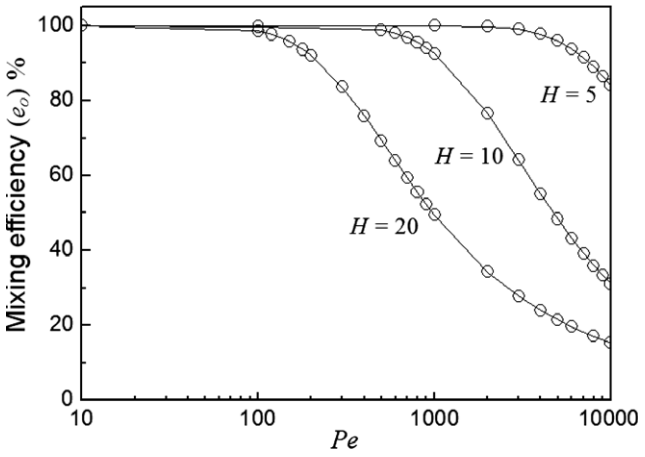

Fig. 15. Effects of Pe on mixing efficiency for the P_7 channel.

efficiency and the flow rate for the P_7 and alternating PM mode systems are illustrated in Fig. 16 as a function of H. In these simulations, the Peclet number is fixed at $Pe = 10^4$. As shown in Fig. 16a, no special mixing modes are needed for the small channel height (H). When H is less than 4, the mixing efficiency is almost 100% for both modes. Around $H = 10$, the alternating PM mode exhibits significantly better mixing efficiency (e_o), but the pure pumping mode (P_7) shows a higher pumping flow rate. For both modes, the flow rate increases linearly with H. The rate of increase of the flow rate with increasing H for the alternating PM mode is half of that for the pure pumping mode.

There have been many micromixers, making use of time-dependent pulsing via secondary channels (Bottausci et al., 2007), staggered herringbone grooves (Stroock et al., 2002), and heterogeneous surface zeta potential (Li, 2004; Erickson and Li, 2002). It is not easy to directly compare the present design with the previous mixers because their conditions (Re, Pe) and methodologies are different. Moreover, our design simultaneously includes mixing and pumping. The comparison of mixing performance is listed in Table 3. The time-dependent pulsing mixing device seems to be the best thanks to the shortest mixing length. However, it has a drawback of using mechanically oscillating syringe pumps, which are not needed in the present AC electroosmotic mixer. Moreover, the staggered herringbone groove and surface heterogeneous zeta potential mixers have drawbacks of long mixing length O(10^4) μm, and high applied DC voltage O(10^2) V/cm, respectively.

Recently, new designs have been proposed for AC electroosmotic pumps using non-planar electrode arrays (Bazant and Ben, 2006; Urbanski et al., 2006). Non-planar electrodes create considerably smooth laminar flow above the steps in a 'fluid conveyor belt' which displays no flow circulations against the main stream. These pumps show faster flow rate and have less tendency for flow reversal, compared with the planar electrodes. No flow circulations give inactive mixing enhancement. However, the flow

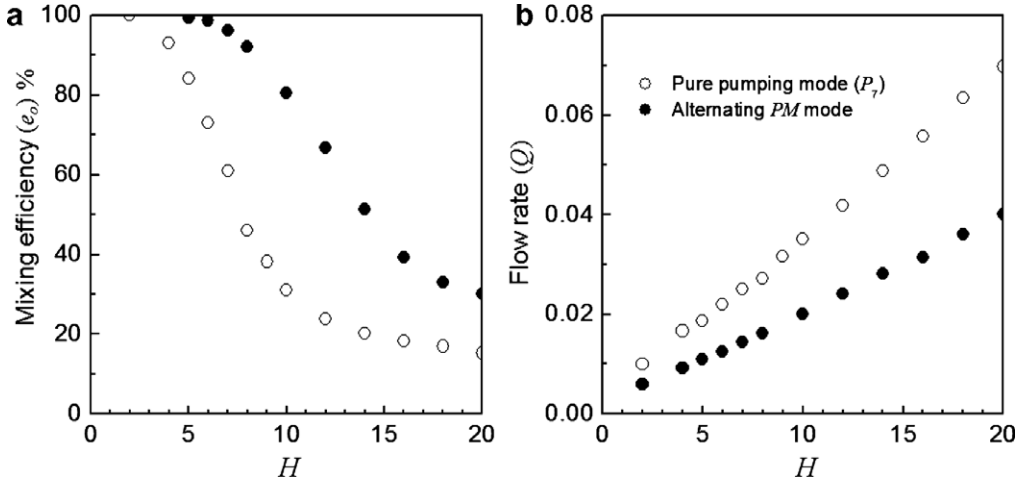

Fig. 16. Effects of mixing efficiency and flow rate on H for $Pe = 10^4$.

Table 3
Comparison of different mixing methods

Mixing method	Cross-sectional size of channels	Re	Pe	Mixing length
Present ($PMPMPMP$)	×50 μm	10^{-1}	10^4	350 μm
Time-dependent pulsing (Bottausci et al., 2007)	100 μm × 200 μm	2.6	5.7×10^5	200 μm
Staggered grooves (Stroock et al., 2002)	85 μm × 200 μm	10^{-2}–10^1	2×10^3–9×10^5	O(10^4) μm
Heterogeneous zeta potential (Erickson and Li, 2002)	50 μm × 50 μm, 25 μm × 25 μm	$<10^{-1}$	–	O(10^3) μm

Erickson and Li (2002) does not explicitly specify the exact values of Re and Pe. The diffusion coefficient D (m^2/s) is of O(10^{-10}).

circulation could be tuned by altering electrode geometries, so it is worth exploiting non-planar electrode arrays for pumping and mixing.

4. Conclusions

A detailed numerical analysis has been performed to elucidate the pumping and mixing modes induced in a microchannel using AC asymmetric electrode arrays. The asymmetric electrode arrays were installed on the top and bottom walls of the channel. The pumping mode was obtained when the sequence of electrode pairs on the top wall was the same as that on the bottom wall, whereas the mixing mode was generated by switching the sequence of the electrode pairs on the top wall. Various combinations of pumping and mixing modes were tested to optimize the channel performance in terms of the mixing efficiency and pumping flow rate. The species equation was solved with the Stokes equation to obtain the concentration and velocity field data. Most of the calculations were performed at $Pe = 10^4$. The results showed that for a given slip velocity, pumping was more effective in channels with smaller heights. For the mixing mode, the shape of the circulation cell was gradually distorted as the top wall position was shifted with respect to the bottom wall. By contrast, such shifting of the relative positions of the top and bottom walls had little effect on the pumping mode. The mixing efficiency (e_o) at the outlet decreased as the Peclet number (Pe) was increased. As the proportion of mixing modes within a sequence of mixing and pumping modes was increased, the flow rate decreased linearly and the mixing efficiency (e_o) increased. Pumping was prohibited in systems with a very large proportion of mixing modes. During each pumping mode, symmetric diverging and converging flow patterns were observed; however, a zigzag motion was observed in the MM' mode. Three mixing modes were obtained: convective circulating motion; diffusive motion arising from forcing the main flow through a narrow region; and diverging flow motion. The alternating PM mode showed good mixing performance throughout the entire calculation domain. As the channel height decreased ($H = 20$, 10 and 5), almost 90% of the mixing efficiency was achieved at large Pe ($Pe = 200$, 1000 and 7000). Systems with a smaller channel height and a smaller Pe exhibited better mixing performance due to the strong diffusion across the channel height.

Acknowledgement

This work was supported by the Creative Research Initiatives of the Korea Science and Engineering Foundation.

References

Ajdari, A., 2000. Pumping liquids using asymmetric electrode arrays. Physical Review E 61 (1), R45–R48.

Bazant, M.Z., Ben, Y., 2006. Theoretical prediction of fast 3D AC electroosmotic pumps. Lab on a Chip 6, 1455–1461.

Bazant, M.Z., Squires, T.M., 2004. Induced-charge electrokinetic phenomena: theory and microfluidic applications. Physical Review Letters 92 (6), 066101.

Beni, G., Tenan, M.A., 1981. Dynamics of electrowetting displays. Journal of Applied Physics 52 (10), 6011–6015.

Bottausci, F., Cardonne, C., Meinhart, C., Mezić, I., 2007. An ultrashort mixing length micromixer: the shear superposition micromixer. Lab on a Chip 7, 396–398.

Brown, A.B.D., Smith, C.G., Rennie, A.R., 2000. Pumping of water with AC electric fields applied to asymmetric pairs of microelectrodes. Physical Review E 63, 016305.

Davis, T.A., Duff, I.S., 1997. An unsymmetric-pattern multifrontal method for sparse LU factorization. SIAM Journal on Matrix Analysis and Applications 18 (1), 140–158.

Erickson, D., Li, D., 2002. Influence of surface heterogeneity on electrokinetically driven microfluidic mixing. Langmuir 18 (5), 1883–1892.

Fuhr, G., Hagedorn, R., Müller, T., Benecke, W., Wagner, B., 1992. Microfabricated electrohydrodynamic (EHD) pumps for liquids of higher conductivity. Journal of Microelectromechanical Systems 1 (3), 141–146.

González, A., Ramos, A., Green, N.G., Castellanos, A., Morgan, H., 2000. Fluid flow induced by nonuniform AC electric fields in electrolytes on microelectrodes. II. A linear double-layer analysis. Physical Review E 61 (4), 4019–4028.

Green, N.G., Ramos, A., González, A., Morgan, H., Castellanos, A., 2000. Fluid flow induced by nonuniform AC electric fields in electrolytes on microelectrodes. I. Experimental measurements. Physical Review E 61 (4), 4011–4018.

Green, N.G., Ramos, A., González, A., Morgan, H., Castellanos, A., 2002. Fluid flow induced by nonuniform AC electric fields in electrolytes on microelectrodes. III. Observation of streamlines and numerical simulation. Physical Review E 66, 026305.

Kataoka, D.E., Troian, S.M., 1999. Patterning liquid flow on the microscopic scale. Nature 402, 794–797.

Kilic, M.S., Bazant, M.Z., Ajdari, A., 2007. Steric effects in the dynamics of electrolytes at large applied voltages. I. Double-layer charging. Physical Review E 75, 021502.

Lastochkin, D.L., Zhou, R., Wang, P., Ben, Y., Chang, H., 2004. Electrokinetic micropump and micromixer design based on AC Faradaic polarization. Journal of Applied Physics 96 (3), 1730–1733.

Li, D., 2004. Electrokinetics in Microfluidics. Elsevier, New-York.

Manz, A., Effenhauser, C.S., Burggraf, N., Harrison, D.J., Seiler, K., Fluri, K., 1994. Electroosmotic pumping and electrophoretic separations for miniaturized chemical analysis systems. Journal of Micromechanics and Microengineering 4, 257–265.

Mpholo, M., Smith, C.G., Brown, A.B.D., 2003. Low voltage plug flow pumping using anisotropic electrode arrays. Sensors and Actuators B 92, 262–268.

Nguyen, N.T., Wereley, S.T., 2003. Fundamentals and Applications of Microfluidics. Artech House, Boston.

Olesen, L.H., Bruus, H., Ajdari, A., 2006. AC electrokinetic micropumps: the effect of geometrical confinement, Faradaic current injection, and nonlinear surface capacitance. Physical Review E 73, 056313.

Ramos, A., Morgan, H., Green, N.G., Castellanos, A., 1999. AC electric-field-induced fluid flow in microelectrodes. Journal of Colloid and Interface Science 217 (2), 420–422.

Ramos, A., González, A., Castellanos, A., Green, N.G., Morgan, H., 2003. Pumping of liquids with AC voltages applied to asymmetric pairs of microelectrodes. Physical Review E 67, 056302.

Squires, T.M., Bazant, M.Z., 2004. Induced-charge electro-osmosis. Journal of Fluid Mechanics 509, 217–252.

Stone, H.A., Stroock, A.D., Ajdari, A., 2004. Engineering flows in small devices: microfluidics towards a lab-on-a-chip. Annual Review of Fluid Mechanics 36, 381–411.

Stroock, A.D., Dertinger, S.K.W., Ajdari, A., Mezić, I., Stone, H.A., Whitesides, G.M., 2002. Chaotic mixer for microchannels. Science 295 (5555), 647–651.

Urbanski, J.P., Levitan, J.A., Burch, D.N., Thorsen, T., Bazant, M.Z., 2006. The effect of step height on the performance of three-dimensional AC electroosmotic microfluidic pumps. Journal of Colloid and Interface Science 309, 332–341.

van Lintel, H.T.G., 1988. A piezoelectric micropump based on micromachining of silicon. Sensors and Actuators A 15, 153–167.

Zhao, H., Bau, H.H., 2007. Microfluidic chaotic stirrer utilizing induced-charge electroosmosis. Physical Review E 75, 066217.